Title

Proper orthogonal decomposition for reduced order dynamic modeling of vapor compression systems

Authors

Ma, Jiacheng
Kim, Donghun
Braun, James E

Publication Date

2021-12-01

DOI

10.1016/j.ijrefrig.2021.09.016

Peer reviewed

Proper Orthogonal Decomposition for Reduced Order Dynamic Modeling of Vapor Compression Systems

Jiacheng Ma[a], Donghun Kim[a,b,*], James E. Braun[a]

[a]*Ray W. Herrick Laboratories, School of Mechanical Engineering, Purdue University, 177 S. Russell Street, West Lafayette, IN, USA*
[b]*Building Technology & Urban Systems Division, Lawrence Berkeley National Laboratory, Berkeley, CA, USA*

Abstract

A computationally efficient but accurate dynamic modeling approach for vapor compression systems is important for many applications. Nonlinear model order reduction techniques which generate reduced order models based on high fidelity vapor compression cycle (VCC) models are attractive for the purposes. In this paper, a number of technical challenges of applying model order reduction methods to VCCs are described and corresponding solution approaches are presented. It starts with a reformulation of a standard finite volume heat exchanger model for matching the baseline model reduction structure. Reduced order models for evaporator and condenser are constructed from numerical snapshots of the high fidelity models using Proper Orthogonal Decomposition (POD). Methodologies for system stability and numerical efficiency of POD reduced order models are described. The reduced order heat exchanger models are then coupled with quasi-static models of other components to form a reduced order cycle model. Transient simulations were conducted over a wide range of operating conditions and results were compared with the full order model as well as measurements. The validation results indicate that the reduced order model can execute much faster than a high-fidelity finite volume model with negligible prediction errors.

Keywords: Model order reduction, Dynamic modeling, Vapor compression cycle, Proper orthogonal decomposition

*Corresponding author
Email address: donghunkim@lbl.gov (Donghun Kim)

Nomenclature

Symbols

$\dot{m}$	Mass flow rate [kg s^{-1}]
$\dot{Q}$	Heat transfer rate [kW]
A	Flow or surface area [m^2]
C_p	Specific heat [kJ $kg^{-1}C^{-1}$]
h	Specific enthalpy [kJ kg^{-1}]
L	Tube length [m]
M	Mass [kg]
P	Pressure [kPa]
T	Temperature [C]
t	Time [s]
u	Specific internal energy [$\mathrm{kJ\,kg^{-1}}$] or control inputs
V	Volume [m^3]
v	Velocity [m s^{-1}]

Greek letters

α	Heat transfer coefficient [$\mathrm{kW\,m^{-2}\,C^{-1}}$]
ρ	Density [$\mathrm{kg\,m^{-3}}$]
τ	Shear stress [$\mathrm{N\,m^{-1}}$]

Subscript

c	Cross-sectional

cwi	Condenser water inlet
ewi	Evaporator water inlet
i	Inlet
o	Outlet
r	Refrigerant
set	Set point
t	Tube
w	Water

1. Introduction

Since transient models for vapor compression cycles (VCC) are particularly important for designing and evaluating control and fault detection diagnostic (FDD) algorithms, transient modeling of VCCs has become an active area of research over past decades. The finite volume (FV) and moving boundary (MB) methods are the two dominant approaches to capture the complex thermo-fluid dynamic behavior of VCCs (Rasmussen, 2012; Rasmussen and Alleyne, 2006; Desideri et al., 2016). The fundamental difference between them is in the discretization schemes for solving the governing conservation equations.

In the literature, the MB method has received significant attention for control applications (He et al., 1998; Rasmussen and Alleyne, 2006, 2004) because of its lower dimensionality and faster execution speed. Bendapudi et al. (2008) presented comparative studies of transient predictions for a chiller system using both methods Pangborn et al. (2015) . However, the model complexity and inherent discontinuities associated with switching model representations when a phase region disappears or reappears can result in simulation failure and limit capability of the MB for advanced control and FDD purposes (Qiao et al., 2016). Recently Kim et al. (2020) presented a general solution to eliminate the discontinuities during mode switches by adopting a Fuzzy modeling approach. However, further studies are needed for better design of membership functions and understanding of the numerical robustness and reliability of this MB approach.

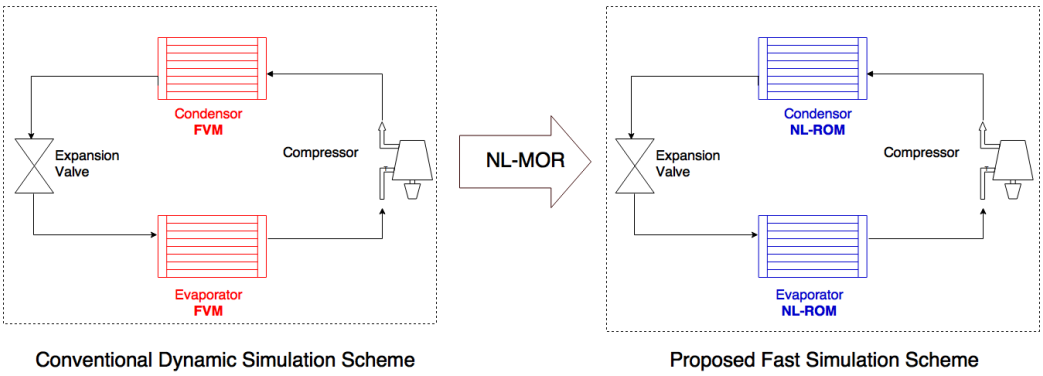

Figure 1: Conceptual diagram of proposed fast simulation approach

In this paper, we present an alternative modeling strategy which applies a well-developed nonlinear model order reduction method (NL-MOR) from other fields (e.g., turbulent flow, applied mathematics and control). The proposed process is depicted in Fig. 1. It starts from a high fidelity dynamic heat exchanger model (denoted as FVM). The proposed approach applies a NL-MOR method to the FVMs in order to generate nonlinear reduced-order models (ROM), and then couples them with quasi-static models of other components to complete a reduced-order VCC model. This approach is attractive since a reduced order VCC model could be extracted from the high fidelity FV models in a systematic manner, and the inherent discontinuities of the MB method can be naturally avoided.

Henrik and Olsson (2005) discussed feasible applications of linear and nonlinear MOR methods for heat exchanger modeling. Linear reduced order models were derived using the balanced truncation and Krylov subspace methods from a linearized heat exchanger model. In addition, a Proper Orthogonal Decomposition (POD) method was applied to produce nonlinear reduced order models. Dynamic responses of those models were compared under a perturbation of the evaporating pressure. It was reported that different models showed similar accuracy and the POD model had the lowest dimension. No comparison of simulation speed was provided. Recently, Xu et al. (2018) developed reduced order heat exchanger models from high-fidelity FV models for an Organic Rankine Cycle using POD. A reduced order evaporator model was implemented for a waste heat recovery system, and its performance was compared with the full order FV model. Simulation results indicated that the reduced order model required less than half the

computation time while providing satisfactory accuracy.

Although the overall idea of applying NL-MOR to VCCs is straightforward, very few studies on this topic can be found in the literature and the few that exist (e.g. Henrik and Olsson (2005); Xu et al. (2018)), resulted in reduced order models that are not generally applicable for most vapor compression and expansion systems because of simplistic assumptions (e.g., fixed refrigerant flow rate and pressure across a heat exchanger). To the knowledge of authors, no previous research has demonstrated the feasibility of applying NL-MOR to a complete VCC model.

This paper 1) describes the major technical challenges of applying a standard NL-MOR to VCC heat exchangers, 2) proposes a series of steps and algorithms to resolve them, 3) demonstrates the feasibility of applying the NL-MOR approach to a complete VCC system, and 4) compares the resulting reduced order VCC model with both a high-fidelity FV model and experimental measurements.

2. Description of Technical Challenges

The objective of NL-MOR methods is as follows. Let $(\boldsymbol{x}, \boldsymbol{u}, \boldsymbol{y})$ be (state, system input, system output) respectively. Given a set of nonlinear ordinary differential equations in the form of

$$\dot{\boldsymbol{x}} = f(\boldsymbol{x}, \boldsymbol{u}), \;\; y = g(\boldsymbol{x}, \boldsymbol{u}), \tag{1}$$

find $\tilde{\boldsymbol{x}}, \tilde{\boldsymbol{f}}, \tilde{\boldsymbol{g}}$ such that

$$\dot{\tilde{\boldsymbol{x}}} = \tilde{f}(\tilde{\boldsymbol{x}}, \boldsymbol{u}), \;\; \boldsymbol{y} = \tilde{g}(\tilde{\boldsymbol{x}}, \boldsymbol{u}), \tag{2}$$

where $\boldsymbol{x} \in \mathbb{R}^N$, $\tilde{\boldsymbol{x}} \in \mathbb{R}^k$ and $k \ll N$.

In other words, NL-MOR seeks to find both dynamic states ($\tilde{\boldsymbol{x}}$) residing in a reduced dimensional space ($k \ll N$) and nonlinear functions ($\tilde{f}, \tilde{g}$) such that input-output responses are preserved (as much as possible).

Although several NL-MOR methods are available and have been popularly used in other scientific fields, significant technical challenges in applying them to heat exchanger modeling were found during this study in addition to the well-known issue of designing input signals, and are summarized as follows.

1. Popular NL-MOR methods, e.g. the proper orthogonal decomposition, cannot be directly applied to a standard FV heat exchanger model structure.

2. (Local) stability of a resulting reduced order model is not guaranteed.
3. Conventional NL-MOR methods implicitly require evaluating all original equations, although the state dimensions are reduced.

Here, the standard FV heat exchanger model means a set of mass and energy balance equations having refrigerant pressure and enthalpies for all control volumes of the heat exchanger as internal states, e.g. Bendapudi et al. (2008). The selection of states eliminates variables of intermediate mass flow rates for control surfaces, and hence it reduces the number of equations.

Those issues and the corresponding solution strategies will be explained in the following sections.

3. Model Order Reduction Methodologies

The Proper Orthogonal Decomposition (POD) method is utilized to generate reduced order heat exchanger models in this paper, which produces optimal low order basis functions from ensembles of data, or namely *snapshots* in the state space. After that, a stabilization method to preserve the stability of the full order model is presented. To address the computational issue, we adopt the discrete empirical interpolation method (DEIM) proposed by Chaturantabut and Sorensen (2010) in this paper which approximates nonlinear functions in conjunction with the POD method.

3.1. Proper Orthogonal Decomposition

A POD reduced order model can inherit the original system dynamics from samples of state trajectories of the baseline model which can be obtained from either a numerical simulation of the full-order model or experimental observations. The nature of the POD is similar to the Fourier modes: functions of interest are projected onto a set of basis functions or modes thus providing a finite set of scalar coefficients that represent the underlying functions. The POD method produces a particular set of modes that form an optimal, orthonormal basis for describing the finite set of samples. More precisely, consider a standard nonlinear system,

$$\dot{\boldsymbol{x}} = f(\boldsymbol{x}, \boldsymbol{u}) \tag{3}$$

where $\boldsymbol{x} \in \mathbb{R}^N$ denotes the dynamic states, $\boldsymbol{u} \in \mathbb{R}^m$ denotes the system inputs. Suppose the system is perturbed with some input profiles, and take

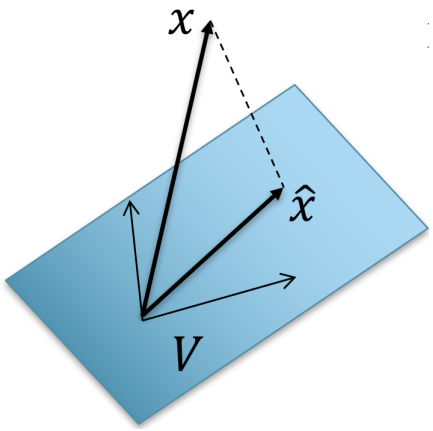

Figure 2: Projection of states vector onto an orthonormal basis.

p snapshots of state responses. Let $\boldsymbol{X}$ be the ensemble of the snapshots as follows,

$$\boldsymbol{X} = \begin{bmatrix} \boldsymbol{x}^{(1)} & \boldsymbol{x}^{(2)} & \dots & \boldsymbol{x}^{(p)} \end{bmatrix} \ (\in \mathbb{R}^{N \times p}), \tag{4}$$

where each column of the snapshots matrix represents states at a time instance.

The POD seeks to find a special basis $\boldsymbol{V_k} (= \begin{bmatrix} \boldsymbol{v}_1 & \boldsymbol{v}_2 & \dots \boldsymbol{v}_k \end{bmatrix} \in \mathbb{R}^{N \times k})$ which solves the following optimization problem:

$$\begin{aligned} &\min \|\boldsymbol{X} - \boldsymbol{V_k}\boldsymbol{V_k}^T\boldsymbol{X}\|_F^2 \\ &\text{s.t.} \quad \boldsymbol{V_k}^T\boldsymbol{V_k} = \boldsymbol{I_k} \end{aligned} \tag{5}$$

where $\|\cdot\|_F$ denotes the Frobenius norm.

The choice of the reduced basis dimension k is certainly of central importance in applying POD, as a trade-off between approximation accuracy and computational savings. Observing the magnitude of singular values can be a natural criterion, since POD approximation error is connected with singular values which are formed in a descent order, as shown in (**??**). Practically, the ratio of amount of energy captured by the POD basis to the total energy is usually used to determine the dimension (Kunisch and Volkwein, 1999; Kerschen et al., 2005; Chaturantabut and Sorensen, 2010),

$$\mathcal{E}(k) = \frac{\sum_{i=1}^{k} \sigma_i^2}{\sum_{i=1}^{N} \sigma_i^2}. \tag{6}$$

where σ_i is the i^{th} singular value of $\boldsymbol{X}$.

A threshold for determining dimension k can be set for the value of $\mathcal{E}(k)$, e.g. 99.99%.

Once the reduced order basis $\boldsymbol{V_k}$ is generated, corresponding POD reduced order models are constructed by applying Galerkin projection. The state space is first approximated by a linear combination of the reduced basis,

$$\boldsymbol{x}(t) \approx \sum_{i=1}^{k} \tilde{x}_i(t)\boldsymbol{v}_i = \boldsymbol{V_k}\tilde{\boldsymbol{x}}(t) \tag{7}$$

where the coefficients vector $\tilde{\boldsymbol{x}} \in \mathbb{R}^k$ will be the reduced states. Then projecting the governing equations of (3) onto the reduced basis results in a reduced system,

$$\dot{\tilde{\boldsymbol{x}}} = \boldsymbol{V_k}^T f(\boldsymbol{V_k}\tilde{\boldsymbol{x}}, \boldsymbol{u}) \tag{8}$$

3.2. Stabilization of POD Reduced Order Models

Preserving the stability of the original high-fidelity model is crucially important for model order reduction methods. Unfortunately, projection-based model order reduction methods, such as the POD, often result in an unstable reduced order model although the baseline system is (locally) stable. There are exceptional cases where, under a certain property of the original system, reduced order models preserve the stability regardless of basis choices (Prajna, 2003). See **??** for more detailed discussions. In practice, this sufficient condition can be used to predict or analyze the stability of a reduced order model as a *prior* knowledge. However, when it is not the case, stabilization methods should follow as a *posterior* process. We adopt the methodology proposed by Amsallem and Farhat (2012). The method is motivated by semidefinite programming (King and Sachs, 2000), and requires primarily the solution of a convex optimization problem.

To describe the approach, let's denote the linearized system description of (8) at an equilibrium point as

$$\boldsymbol{V_k}\dot{\tilde{\boldsymbol{x}}} = \boldsymbol{A}\boldsymbol{V_k}\tilde{\boldsymbol{x}}. \tag{9}$$

For stability analysis and notational simplicity, the term associated with inputs is omitted. Let's consider another k-dimensional subspace represented by $\boldsymbol{W_k}$ ($\in \mathbb{R}^{N\times k}$) where each column vector of $\boldsymbol{W_k}$ indicates a basis vector

of the new subspace[1]. The projection of the dynamics of (8) onto it forms new dynamics described as follows.

$$\boldsymbol{W}_k^T \boldsymbol{V}_k \dot{\tilde{\boldsymbol{x}}} = \boldsymbol{W}_k^T \boldsymbol{A} \boldsymbol{V}_k \tilde{\boldsymbol{x}} \tag{10}$$

According to the Lyapunov stability theorem for a LTI descriptor system, the (asymptotic) stability criteria can be written as

$$\boldsymbol{V}_k^T \boldsymbol{W}_k \boldsymbol{P} \boldsymbol{W}_k^T \boldsymbol{A} \boldsymbol{V}_k + \boldsymbol{V}_k^T \boldsymbol{A}^T \boldsymbol{W}_k \boldsymbol{P} \boldsymbol{W}_k^T \boldsymbol{V}_k \prec \boldsymbol{0}. \tag{11}$$

The main idea of the stabilization method is to find $\boldsymbol{W_k}$ which minimizes the deviation from the POD subspace, i.e. $\boldsymbol{V_k}$, while aiming at preserving the asymptotic stability of the newly projected system (10).

Given a matrix $\boldsymbol{Y}_{k+p} \in \mathbb{R}^{N \times (k+p)}$, $\boldsymbol{W_k}$ can be parameterized as

$$\boldsymbol{W}_k = \boldsymbol{Y}_{k+p} \boldsymbol{Z}, \tag{12}$$

where $\boldsymbol{Z} \in \mathbb{R}^{(k+p) \times k}$ is the coordinates of $\boldsymbol{W_k}$ with respect to $\boldsymbol{Y}_{k+p}$. Theoretically $\boldsymbol{Y}_{k+p}$ could be any matrix in $\mathbb{R}^{N \times (k+p)}$ but it is natural to choose the first $k+p$ ($\leq N$) column vectors of $\boldsymbol{V}$ in (**??**), since it is optimal to represent the empirical data.

Then, the stability constraint (11) can be written as

$$\boldsymbol{V}_k^T \boldsymbol{Y}_{k+p} \boldsymbol{Z} \boldsymbol{P} \boldsymbol{Z}^T \boldsymbol{Y}_{k+p}^T \boldsymbol{A} \boldsymbol{V}_k + \boldsymbol{V}_k^T \boldsymbol{A}^T \boldsymbol{Y}_{k+p} \boldsymbol{Z} \boldsymbol{P} \boldsymbol{Z}^T \boldsymbol{Y}_{k+p}^T \boldsymbol{V}_k \prec \boldsymbol{0}. \tag{13}$$

Note that constraint (13) is a Quadratic Matrix Inequality in the variable $\boldsymbol{Z}$ which can not be solved by convex solvers (Boyd et al., 1994). In order to apply techniques from convex optimization, the change of variable

$$\tilde{\boldsymbol{P}} = \boldsymbol{Z} \boldsymbol{P} \boldsymbol{Z}^T \tag{14}$$

is introduced, which leads to a Linear Matrix Inequality.

With this parameterization, the objective function can be expressed as

$$f(\boldsymbol{Z}) = \|\boldsymbol{Y}_{k+p} \boldsymbol{Z} - \boldsymbol{V}_k\| \tag{15}$$

where $\|\cdot\|$ denotes any matrix norm. It was proved in Amsallem and Farhat (2012) that if there exists a positive definite matrix $\hat{\boldsymbol{P}} \in \mathbb{R}^{(k+p) \times (k+p)}$ which

[1]The basis does not need to be orthonormal.

can be partitioned in blocks as

$$\hat{\boldsymbol{P}} = \begin{bmatrix} \hat{\boldsymbol{P}}_{11} & \hat{\boldsymbol{P}}_{12} \\ \hat{\boldsymbol{P}}_{12}^T & \hat{\boldsymbol{P}}_{22} \end{bmatrix} \tag{16}$$

where $\hat{\boldsymbol{P}}_{11} \in \mathbb{R}^{k\times k}$, then a solution to the minimization problem of (15) constrained by (13) can be constructed as

$$\tilde{\boldsymbol{P}} = \begin{bmatrix} \hat{\boldsymbol{P}}_{11} \\ \hat{\boldsymbol{P}}_{12}^T \end{bmatrix} \hat{\boldsymbol{P}}_{11}^{-1} \begin{bmatrix} \hat{\boldsymbol{P}}_{11} & \hat{\boldsymbol{P}}_{12} \end{bmatrix}. \tag{17}$$

Therefore, it follows that

$$\boldsymbol{Z} = \begin{bmatrix} \hat{\boldsymbol{P}}_{11} \\ \hat{\boldsymbol{P}}_{12}^T \end{bmatrix}. \tag{18}$$

In practice, the optimization problem of interest can be directly solved using convex optimization packages, e.g. CVX (Grant and Boyd, 2014).

It is important to mention that it is possible that no feasible solution exists for all $p \in \{0, \cdots, N-k\}$ to this problem. That is, although the method in general increases the chance of obtaining a stable reduced order model substantially, it might fail for doing that depending on the dynamics of the original system $\boldsymbol{A}$ and the POD basis $\boldsymbol{V}_k$. In that case, the only option is to attempt modifying $\boldsymbol{V}_k$ through trials and errors.

3.3. Discrete Empirical Interpolation Method

The standard POD model reduction technique reduces the dimension of internal states, and is computationally efficient for LTI systems (Kalashnikova et al., 2014). However, when dealing with a system of general nonlinear ordinary differential equations (ODEs), the computational complexity of evaluating the full order nonlinear equations remains even though the number of states is reduced, as discussed in Section 2. We adopt the solution proposed by Chaturantabut and Sorensen (2010), namely the discrete empirical interpolation method (DEIM), which has been successfully applied to improve computational efficiency of projection-based nonlinear reduced order models. It constructs specially selected interpolation indices to minimize a certain upper bound of the approximation error. It is applicable to ODEs arising from finite difference or finite volume discretization of time dependent

partial differential equations (PDEs). The DEIM approach can be viewed as a combination of projection and interpolation. The nonlinear functions, i.e. f in (3), are approximated by projecting them onto a reduced basis of dimension $m \ll N$. Recall that the POD basis is generated from snapshots of state trajectories. The same procedure is adopted to extract a subspace from snapshots of nonlinear dynamics:

$$\boldsymbol{F} = \begin{bmatrix} \boldsymbol{f}^{(1)} & \boldsymbol{f}^{(2)} & \dots & \boldsymbol{f}^{(q)} \end{bmatrix} \in \mathbb{R}^{N \times q}. \tag{19}$$

It should be noted that the snapshots of nonlinear functions can be obtained from the POD procedure, and hence no additional computational cost is added to the original POD procedure although more computer memory is required to store values of nonlinear functions during simulation. Nonlinear functions are approximated by projection onto a reduced basis

$$\boldsymbol{f}(t) \approx \boldsymbol{T}\boldsymbol{c}(t) \tag{20}$$

where $\boldsymbol{T} \in \mathbb{R}^{N \times m}$ is obtained by applying POD to the nonlinear function snapshots matrix $\boldsymbol{F}$ in (19), and $\boldsymbol{c} \in \mathbb{R}^m$ represents the vector of corresponding time coefficients. To calculate the coefficients from the overdetermined system in (20), m distinguished rows are selected to form a well-posed system. Consider an interpolation scheme:

$$\boldsymbol{P}^T\boldsymbol{f}(t) \approx \boldsymbol{P}^T\boldsymbol{T}\boldsymbol{c}(t) \tag{21}$$

where $\boldsymbol{P}$ is a matrix whose i^{th} column $\boldsymbol{e}_{\zeta_i}$ is identified by an interpolation index ζ_i, which means $\boldsymbol{e}_{\zeta_i} = \begin{bmatrix} 0 & \dots & 0 & 1 & 0 \dots & 0 \end{bmatrix}^T$ contains the ζ_i^{th} columns of the identity matrix $\boldsymbol{I} \in \mathbb{R}^{N \times N}$,

$$\boldsymbol{P} = \begin{bmatrix} \boldsymbol{e}_{\zeta_1} & \boldsymbol{e}_{\zeta_2} & \dots & \boldsymbol{e}_{\zeta_m} \end{bmatrix}. \tag{22}$$

Suppose $\boldsymbol{P}^T\boldsymbol{T}$ is nonsingular, then the coefficients can be uniquely determined,

$$\boldsymbol{c}(t) = (\boldsymbol{P}^T\boldsymbol{T})^{-1}\boldsymbol{P}^T\boldsymbol{f}(t). \tag{23}$$

The final interpolation approximation of the nonlinear functions is expressed as

$$\tilde{\boldsymbol{f}}(t) = \boldsymbol{T}(\boldsymbol{P}^T\boldsymbol{T})^{-1}\boldsymbol{P}^T\boldsymbol{f}(t). \tag{24}$$

Note that $\boldsymbol{P}$ and $\boldsymbol{T}$ are constant matrices, so the matrix multiplication can be pre-computed before the online simulation. $\boldsymbol{P}^T\boldsymbol{f}(t)$ can be viewed as the evaluation of a partial set of functions from the original high order system at the specified interpolation indices, which will significantly reduce the computational load. To complete the DEIM, Chaturantabut and Sorensen (2010) proposed an algorithm for determining interpolation indices (matrix $\boldsymbol{P}$) inductively from the basis $\boldsymbol{T}$. Interpolation indices are selected to limit growth of an error bound, and are guaranteed to be hierarchical and non-repeated. An approximated error bound was derived for the DEIM algorithm in Chaturantabut and Sorensen (2010):

$$\left\|\boldsymbol{f}-\tilde{\boldsymbol{f}}\right\|_2 \approx \left\|(\boldsymbol{P}^T\boldsymbol{T})^{-1}\right\|_2 \sigma_{m+1} \tag{25}$$

where σ_{m+1} is the $(m+1)^{th}$ leading singular value of the nonlinear snapshots matrix in (19). In practice, it can be used in determining the number of interpolation points. As more functions are evaluated, the approximation error is smaller since singular values are arranged in a descending order by SVD. When there is a significant gap between the magnitude of two adjacent singular values, the number of indices m could be selected at that point.

4. Reduced Order Modeling for VCC

This section presents a nonlinear model order reduction framework for heat exchanger models. A reformulated finite volume (FV) heat exchanger model is introduced by choosing a different pair of thermodynamic states, and then discretized with a staggered grid. After that, the POD in conjunction with the DEIM approach is used to generate reduced order models. Finally numerical treatments are described to improve model robustness.

4.1. Reformulation of Finite Volume Model

As mentioned in Section 2 to enable the use of nonlinear model order reduction techniques, a typical FV model (Bendapudi et al., 2008; Rasmussen, 2012), which applies refrigerant pressure and enthalpies as dynamic states, needs to be converted to the standard ODE form as shown in (3). This is because the FV formulation consisting of refrigerant pressure and enthalpies as states as well as an elimination of interface mass flow rates, has a descriptor form $\boldsymbol{E}(\boldsymbol{x})\dot{\boldsymbol{x}} = \boldsymbol{f}(\boldsymbol{x},\boldsymbol{u})$ due to the partial derivatives of refrigerant density with respect to pressure and enthalpy in the mass balance and energy

balance. This model structure (denoted as the standard FV model in this paper) can not be used as for the baseline nonlinear model reduction. Therefore a reformulated FV model selecting refrigerant density, internal energy and interface mass flow rates as dynamic states was developed. A momentum balance is integrated into the governing equations to evaluate dynamics of refrigerant mass flow rates.

The system of PDEs can be solved by discretizing spatially and then integrating in the time domain. The heat exchanger is divided into $\boldsymbol{n}$ equal control volumes. Integrating the governing equations over the length of each control volume yields a system of ODEs:

$$\frac{d\rho_j}{dt} = \frac{1}{V_j}(\dot{m}_k - \dot{m}_{k+1}) \tag{26}$$

$$\frac{d\dot{m}_k}{dt} = \frac{1}{L}\left(\dot{m}_{j-1}v_{j-1} - \dot{m}_j v_j + A_c(P_{j-1} - P_j) - F_f\right) \tag{27}$$

$$\frac{du_j}{dt} = \frac{1}{V_j\rho_j}\left(\dot{m}_k h_{j-1} - \dot{m}_{k+1}h_j - \dot{Q}_{r,j} + u_j(\dot{m}_{k+1} - \dot{m}_k)\right) \tag{28}$$

$$\frac{dT_{t,j}}{dt} = \frac{\dot{Q}_{r,j} - \dot{Q}_{w,j}}{M_{t,j}C_{pt}} \tag{29}$$

$$\frac{dT_{w,j}}{dt} = \frac{\dot{m}_w C_{pw}(T_{w,j+1} - T_{w,j}) + \dot{Q}_{w,j}}{M_{w,j}C_{pw}} \tag{30}$$

A staggered grid scheme was utilized to derive the above equations which has been commonly used in dynamic modeling of thermo-fluid systems to decouple the momentum balance from the mass and energy balances (Elmqvist et al., 2003; Laughman and Qiao, 2019). As shown in Fig. 3, equations of refrigerant mass and energy balances (indices j) are solved in the volume cells (solid black line), and the momentum balances (indices k) are solved in the flow cells (dashed blue line), which are staggered by half of one volume cell. For the reformulated FV heat exchanger model, the dynamic states are

$$\boldsymbol{x} = \left[\rho_1, \ldots, \rho_n, \dot{m}_1, \ldots, \dot{m}_n, u_1, \ldots, u_n, T_{t,1} \ldots, T_{t,n}, T_{w,1}, \ldots, T_{w,n}\right]^T \tag{31}$$

$$= \left[\boldsymbol{\rho}, \boldsymbol{m}, \boldsymbol{u}, \boldsymbol{T}\right]^T (\in \mathbb{R}^{5\times n}), \tag{32}$$

and inputs or boundary conditions to the heat exchanger model consist of refrigerant inlet mass flow rate and enthalpy $(\dot{m}_i, h_i)$, outlet pressure (P_o), and the inlet mass flow rate and temperature of the secondary fluid,

$$\left[\dot{m}_i, h_i, P_o, \dot{m}_{wi}, T_{wi}\right]^T \tag{33}$$

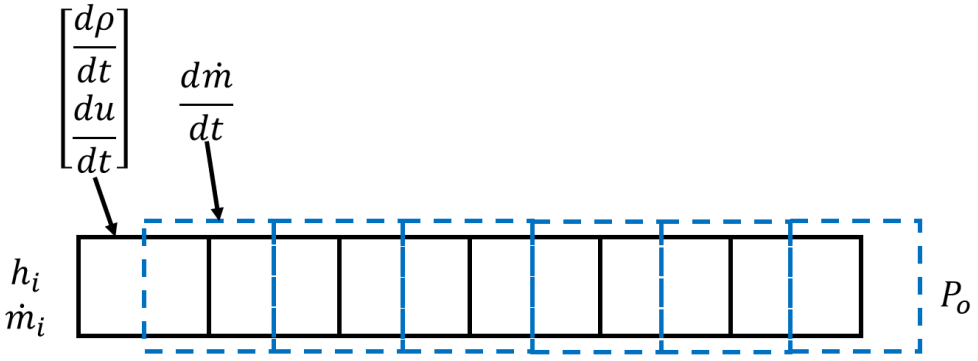

Figure 3: Staggered grid for heat exchanger discretization.

Refrigerant pressure and enthalpy are evaluated as functions of density and internal energy of each control volume $P_j(\rho_j, u_j), h_j(\rho_j, u_j)$. For those evaluations, tabular or regression approaches may be utilized based on a pressure and enthalpy database obtained from REFPROP or CoolProp (Lemmon et al., 2010; Bell et al., 2014).

4.2. POD-DEIM Heat Exchanger Model

Each dynamic state of the reformulated heat exchanger model consists of refrigerant density, mass flow rate, internal energy, tube temperature and secondary fluid temperature for each control volume as shown in (31). Snapshots of the state trajectories as well as nonlinear functions are taken from the numerical simulation of the full-order model under a perturbation of inputs. Reduced order heat exchanger models are constructed using the POD and stabilization methods introduced in Section 3. However no solution to the stabilization problem was found (see the last paragraph of Section 3.2), and therefore we attempted to modify the POD basis to resolve this issue as described below.

Instead of directly applying the POD method to the entire state trajectory matrix, it was split into four matrices according to the thermodynamic and fluid properties of $\boldsymbol{\rho}, \boldsymbol{m}, \boldsymbol{u}$ and $\boldsymbol{T}$ (see (31)), and then the POD was applied to each sub-matrix. This results in four sets of reduced order basis corresponding to the different physical properties as follows.

$$\boldsymbol{\rho} \approx \boldsymbol{V}_\rho \tilde{\boldsymbol{\rho}} \quad \dot{\boldsymbol{m}} \approx \boldsymbol{V}_m \tilde{\dot{\boldsymbol{m}}} \quad \boldsymbol{u} \approx \boldsymbol{V}_u \tilde{\boldsymbol{u}} \quad \boldsymbol{T} \approx \boldsymbol{V}_T \tilde{\boldsymbol{T}} \tag{34}$$

where $\boldsymbol{T} = \begin{bmatrix} \boldsymbol{T}_t^T & \boldsymbol{T}_w^T \end{bmatrix}^T$, and the resulting reduced states are

$$\tilde{\boldsymbol{x}} = \begin{bmatrix} \tilde{\boldsymbol{\rho}}^T & \tilde{\boldsymbol{m}}^T & \tilde{\boldsymbol{u}}^T & \tilde{\boldsymbol{T}}^T \end{bmatrix}^T. \tag{35}$$

A linearized model at an equilibrium point[2] is

$$\begin{bmatrix} \boldsymbol{V}_\rho & & & \boldsymbol{0} \\ & \boldsymbol{V}_u & & \\ & & \boldsymbol{V}_m & \\ \boldsymbol{0} & & & \boldsymbol{V}_T \end{bmatrix} \begin{bmatrix} \dot{\tilde{\boldsymbol{\rho}}} \\ \dot{\tilde{\boldsymbol{m}}} \\ \dot{\tilde{\boldsymbol{u}}} \\ \dot{\tilde{\boldsymbol{T}}} \end{bmatrix} = \boldsymbol{A} \begin{bmatrix} \boldsymbol{V}_\rho & & & \boldsymbol{0} \\ & \boldsymbol{V}_u & & \\ & & \boldsymbol{V}_m & \\ \boldsymbol{0} & & & \boldsymbol{V}_T \end{bmatrix} \begin{bmatrix} \tilde{\boldsymbol{\rho}} \\ \tilde{\boldsymbol{m}} \\ \tilde{\boldsymbol{u}} \\ \tilde{\boldsymbol{T}} \end{bmatrix}. \tag{36}$$

For the system of (36), it becomes possible to obtain a stabilizing basis $\boldsymbol{W_k}$ (see (10)) by applying the stabilization method directly on (36). However, for numerical reasoning, we narrowed down $\boldsymbol{W_k}$ (see (10)) as

$$\boldsymbol{W_k} = \begin{bmatrix} \boldsymbol{I} & & & \boldsymbol{0} \\ & \boldsymbol{I} & & \\ & & \boldsymbol{I} & \\ \boldsymbol{0} & & & \boldsymbol{W}_T \end{bmatrix}, \tag{37}$$

and searched the unknown $\boldsymbol{W}_T$ in the range of POD basis generated from $\boldsymbol{V_T}$ to stabilize (36).

The final stabilized reduced system has the following form.

$$\begin{bmatrix} \boldsymbol{I} & & & \boldsymbol{0} \\ & \boldsymbol{I} & & \\ & & \boldsymbol{I} & \\ \boldsymbol{0} & & & \boldsymbol{W}_T^T \boldsymbol{V}_T \end{bmatrix} \begin{bmatrix} \dot{\tilde{\boldsymbol{\rho}}} \\ \dot{\tilde{\boldsymbol{m}}} \\ \dot{\tilde{\boldsymbol{u}}} \\ \dot{\tilde{\boldsymbol{T}}} \end{bmatrix} = \begin{bmatrix} \boldsymbol{V}_\rho^T & & & \boldsymbol{0} \\ & \boldsymbol{V}_u^T & & \\ & & \boldsymbol{V}_m^T & \\ \boldsymbol{0} & & & \boldsymbol{W}_T^T \end{bmatrix} \boldsymbol{f}\Big(\begin{bmatrix} \boldsymbol{V}_\rho & & & \boldsymbol{0} \\ & \boldsymbol{V}_u & & \\ & & \boldsymbol{V}_m & \\ \boldsymbol{0} & & & \boldsymbol{V}_T \end{bmatrix} \begin{bmatrix} \tilde{\boldsymbol{\rho}} \\ \tilde{\boldsymbol{m}} \\ \tilde{\boldsymbol{u}} \\ \tilde{\boldsymbol{T}} \end{bmatrix} \Big), \tag{38}$$

or more compactly

$$\boldsymbol{W_k}^T \boldsymbol{V_k} \dot{\tilde{\boldsymbol{x}}} = \boldsymbol{W_k}^T \boldsymbol{f}(\boldsymbol{V_k} \tilde{\boldsymbol{x}}, \boldsymbol{B}). \tag{39}$$

Finally, the DEIM approximation is applied to the reformulated heat exchanger model to reduce the computational cost that depends on the full

[2]The term associated with inputs is not shown since it is not used for stability analysis.

order nonlinear functions in the reduced order model (39). Similar to splitting the state trajectories snapshots, the nonlinear function snapshots are grouped based on reduced states shown in (35). Then interpolation indices are constructed for each group of equations. Note that refrigerant mass balances are linear in refrigerant mass flow rates, thus there is no need to apply the DEIM approximation, and the number of reduced mass balances to be evaluated completely depends on the dimension of refrigerant density basis $\boldsymbol{V}_\rho$. As shown in (25), the DEIM approximation error bound is indicted by singular values of the snapshots matrix. Therefore, the ratio of energy captured by the POD basis can also be adopted here to determine the number of interpolation points.

The overall sequence of the POD-DEIM scheme is summarized in Fig. 4.

5. Feasibility Demonstration, Performance and Further Investigation

The proposed methodology was applied to a R134a centrifugal chiller system which consists of shell-and-tube condenser and evaporator, single stage centrifugal compressor, thermostatic expansion valve (TXV), and local controller adjusting the compressor's inlet guide vane for capacity control. The system description, a system model based on the standard FV heat exchanger formulation and validation with experimental data for the system are presented in (Bendapudi et al., 2008).

To show the feasibility, accuracy and computational benefit of the proposed methodology, it was applied to the chiller system and the resulting reduced order model was compared with 1) the standard FV-based model, 2) full-order reformulated model, and 3) experimental data over a wide range of operating conditions. The timeseries dataset consists of a series of step tests performed on the chiller system over 26 operating conditions where the step inputs are water inlet temperatures for condenser and evaporator, and the chilled water temperature set point. See Fig. 5 for the step test input signals.

Comparisons between two reduced order models obtained from different snapshots were also investigated in this section. For this, two data sets were extracted from the timeseries data. One, namely **ROM(4)**, is associated with the first four operating conditions out of the 26 operating conditions, while the other, namely **ROM(9)**, corresponds to the first nine operating

conditions (see Fig. 5). Each data set includes profiles of refrigerant inlet mass flow rate, inlet enthalpy, outlet pressure, and the inlet mass flow rate and temperature of the secondary fluid for condenser and evaporator, which are the inputs to the reformulated heat exchanger models as shown in (33). The profiles for each scenario were fed to the reformulated full-order heat exchanger models (15 control volumes) to generate snapshots of state and function trajectories for the POD and DEIM processes. The simulations were carried out in the Dymola environment with the Radau IIa solver and default relative error tolerance of 10^{-4}.

5.1. Generation of Reduced Order Vapor Compression Cycle Model

The approach described in Section 4.2 was applied to the snapshot matrices for each scenario of ROM(4) and ROM(9). Remember that we apply the POD method to the dynamics of $\boldsymbol{\rho}, \boldsymbol{m}, \boldsymbol{u}$ and $\boldsymbol{T}$ individually resulting in four sets of reduced order bases, i.e., $\boldsymbol{V}_\rho, \boldsymbol{V}_m, \boldsymbol{V}_u, \boldsymbol{V}_T$ in (34). The reduced order dimension of each subspace was chosen by looking at the energy ratio defined by (6). The threshold of 99.99% was uniformly applied. Values of the energy captured by each mode of the reduced space ($\sigma_k^2/\sum_{i=1}^{N}\sigma_i^2,\ k = 1:n$) for the condenser of ROM(9) are shown in Fig. 6.

Fig. 7 shows energy of modes of the nonlinear function snapshot matrices. The number of refrigerant momentum balances, energy balances, and tube and water energy balances for the reduced order model were selected based on the criteria that the reduced bases of nonlinear functions capture 99.9% of the total energy. The final POD-DEIM reduced order condenser and evaporator models are summarized in Table. 1. It can be seen that for the ROM(4) more than half of the states are reduced and roughly one third of the nonlinear ODEs are eliminated by the DEIM scheme. On the other hand, the ROM(9) leads to less reduction in states and ODEs. This is because the ROM(9) covers a wider range of operating conditions which would require additional dimensions to explain them.

The reduced order condenser and evaporator models were coupled with quasi-static models of the compressor and TXV, and the controller model to form a reduced cycle model. The inputs to the complete cycle model consist of water inlet temperatures and flow rates for condenser and evaporator, and the chilled water set point temperature.

Table 1: Reduced order condenser and evaporator models

HX	Cond States	Cond ODEs	Evap States	Evap ODEs
Full order	75	75	75	75
POD-DEIM ROM(4)	34	53	32	53
POD-DEIM ROM(9)	43	61	38	66

5.2. Result Comparisons

The reduced order cycle models for ROM(4) and ROM(9) respectively, were simulated to predict cycle transient responses over the 26 operating conditions. The two baseline models for comparisons are 1) the standard FV-based model utilizing refrigerant pressure and enthalpy as states, namely FV Ph, and 2) the full-order reformulated FV model, namely FOM. Remember that ROM(4) and ROM(9) were generated from a part of the 26 operating conditions. Therefore inputs and trajectories for the rest of the conditions were unexplored in generating the reduced order models.

Fig. 8 to 11 show result comparisons of refrigerant condensing and evaporating pressures, water exit temperatures, motor power, and heat exchanger loads for all models over the 26 operating conditions. The results show that the FV-Ph and FOM are nearly identical and that they agree well with the measurements. Discrepancies between the ROMs and measurements are typically observed for the operating conditions that were not included in the generation of the ROMs, that is after 4 hours. This makes sense because the limited input perturbations are likely not sufficient to simulate dynamics that cover the entire *controllable subspace*. Nonetheless, the ROMs are still capable of capturing the essential features of the chiller system. It can be clearly seen that the ROM(9) yields a higher accuracy than ROM(4) in predicting the condensing pressure, motor power, and condenser load. Fig. 12 shows the normalized error residuals (NER) (Pangborn et al., 2015) for the ROMs which were computed by

$$\text{NER} = \frac{\sum_{k=1}^{t}(y_{\text{predicted}}(k) - y_{\text{measured}}(k))^2}{\sum_{k=1}^{t}(y_{\text{measured}}(k))^2}. \tag{40}$$

It was observed that predictions of the motor power using the reduced order models had significant discrepancies compared to measurements. This

is because the compressor model, specifically the refrigerant flow rate map, is sensitive to the refrigerant pressures. Errors in the compressor inlet guide vane controller model amplified prediction errors of the refrigerant mass flow rate. Large value of NER in the condenser load was due to prediction errors of refrigerant properties, e.g. condensing pressure (Fig. 8). However, clearly a significant reduction in NER can be observed from ROM(4) to ROM(9).

Simulation speed is measured by the real time factor (RTF) (Pangborn et al., 2015):

$$\text{RTF} = \frac{\textit{length of CPU time taken to run simulation}}{\textit{length of time that is simulated}}. \tag{41}$$

For real-time simulation applications, a model having RTF less than 1 is generally required. Simulation speed of the ROMs, FOM, and FV-Ph are shown in Table. 2. The total number of dynamic states and ODEs to be solved for each model are also displayed, since they play an important role in determining the model execution speed. It can be seen that all these models run faster than the real time. Compared with the FOM, the ROM(4) and ROM(9) require less than half the computation times. ROM(9) requires about 28% more simulation time than ROM(4). This confirms the trade-off between the computational efficiency and accuracy.

Table 2: Simulation speed comparison

Simulation	No. States	No. ODEs	RTF
Standard FV (P,h)	92	92	0.03
Reformulated FOM	150	150	0.0137
ROM (4)	66	106	0.005
ROM (9)	81	127	0.0064

It is interesting to see that the FV-Ph has the lowest number of ODEs but resulted in the highest computation time. This is attributed to the model structure. Although the FOM consists of more states and ODEs because of the inclusion of the momentum balance, it has a standard ODE form as shown in Section 4.1. The FV-Ph model has the descriptor form as mentioned in Section 2 and matrix inversion is carried out at each time step of the numerical integration, which is computationally expensive.

6. Conclusions

This paper described unique challenges for modeling a complete vapor compression and expansion system when applying nonlinear model order reduction methods, and presented a series of methodologies to overcome those issues. The feasibility of applying the nonlinear model order reduction method to refrigeration cycle systems for a centrifugal chiller was presented. Using the POD-DEIM model reduction scheme, dynamic states as well as differential equations to be solved were reduced, leading to an 80% computation time reduction compared to a standard finite volume modeling approach.

Acknowledgments

This work was supported by the Center for High Performance Buildings (CHPB) at Purdue University.

References

Amsallem, D., Farhat, C., 2012. Stabilization of projection-based reduced-order models. International Journal for Numerical Methods in Engineering 91 (4), 358–377.

Bell, I. H., Wronski, J., Quoilin, S., Lemort, V., 2014. Pure and pseudo-pure fluid thermophysical property evaluation and the open-source thermophysical property library coolprop. Industrial & engineering chemistry research 53 (6), 2498–2508.

Bendapudi, S., Braun, J. E., Groll, E. A., 2008. A comparison of moving-boundary and finite-volume formulations for transients in centrifugal chillers. International journal of refrigeration 31 (8), 1437–1452.

Boyd, S., El Ghaoui, L., Feron, E., Balakrishnan, V., 1994. Linear matrix inequalities in system and control theory. Vol. 15. Siam.

Chaturantabut, S., Sorensen, D. C., 2010. Nonlinear model reduction via discrete empirical interpolation. SIAM Journal on Scientific Computing 32 (5), 2737–2764.

Desideri, A., Dechesne, B., Wronski, J., Van den Broek, M., Gusev, S., Lemort, V., Quoilin, S., 2016. Comparison of moving boundary and finite-volume heat exchanger models in the modelica language. Energies 9 (5), 339.

Elmqvist, H., Tummescheit, H., Otter, M., 2003. Object-oriented modeling of thermo-fluid systems. In: 3rd International Modelica Conference. pp. 269–286.

Grant, M., Boyd, S., 2014. Cvx: Matlab software for disciplined convex programming, version 2.1.

He, X.-D., Liu, S., Asada, H. H., Itoh, H., 1998. Multivariable control of vapor compression systems. HVAC&R Research 4 (3), 205–230.

Henrik, K., Olsson, A., 2005. Model order reduction of a heat exchanger model.

Kalashnikova, I., Arunajatesan, S., Barone, M. F., van Bloemen Waanders, B. G., Fike, J. A., 2014. Reduced order modeling for prediction and control of large-scale systems. Sandia National Laboratories Report, SAND (2014-4693).

Kerschen, G., Golinval, J.-c., Vakakis, A. F., Bergman, L. A., 2005. The method of proper orthogonal decomposition for dynamical characterization and order reduction of mechanical systems: an overview. Nonlinear dynamics 41 (1-3), 147–169.

Kim, D., Ma, J., Braun, J. E., Groll, E. A., 2020. Fuzzy modeling approach for transient vapor compression and expansion cycle simulation. International Journal of Refrigeration.

King, B. B., Sachs, E. W., 2000. Semidefinite programming techniques for reduced order systems with guaranteed stability margins. Computational Optimization and Applications 17 (1), 37–59.

Kunisch, K., Volkwein, S., 1999. Control of the burgers equation by a reduced-order approach using proper orthogonal decomposition. Journal of optimization theory and applications 102 (2), 345–371.

Laughman, C. R., Qiao, H., 2019. On closure relations for dynamic vapor compression cycle models. In: Proceedings of The American Modelica Conference 2018, October 9-10, Somberg Conference Center, Cambridge MA, USA. No. 154. Linköping University Electronic Press, pp. 67–76.

Lemmon, E., Huber, M., McLinden, M., 2010. Nist standard reference database 23, reference fluid thermodynamic and transport properties (refprop), version 9.0, national institute of standards and technology. R1234yf. fld file dated December 22, 2010.

Pangborn, H., Alleyne, A. G., Wu, N., 2015. A comparison between finite volume and switched moving boundary approaches for dynamic vapor compression system modeling. International Journal of Refrigeration 53, 101–114.

Prajna, S., 2003. Pod model reduction with stability guarantee. In: 42nd IEEE International Conference on Decision and Control (IEEE Cat. No. 03CH37475). Vol. 5. IEEE, pp. 5254–5258.

Qiao, H., Laughman, C. R., Aute, V., Radermacher, R., 2016. An advanced switching moving boundary heat exchanger model with pressure drop. International journal of refrigeration 65, 154–171.

Rasmussen, B. P., 2012. Dynamic modeling for vapor compression systemspart i: Literature review. HVAC&R Research 18 (5), 934–955.

Rasmussen, B. P., Alleyne, A. G., 2004. Control-oriented modeling of transcritical vapor compression systems. J. Dyn. Sys., Meas., Control 126 (1), 54–64.

Rasmussen, B. P., Alleyne, A. G., 2006. Dynamic modeling and advanced control of air conditioning and refrigeration systems. Tech. rep., Air Conditioning and Refrigeration Center. College of Engineering .

Xu, B., Yebi, A., Hoffman, M., Onori, S., 2018. A rigorous model order reduction framework for waste heat recovery systems based on proper orthogonal decomposition and galerkin projection. IEEE Transactions on Control Systems Technology.

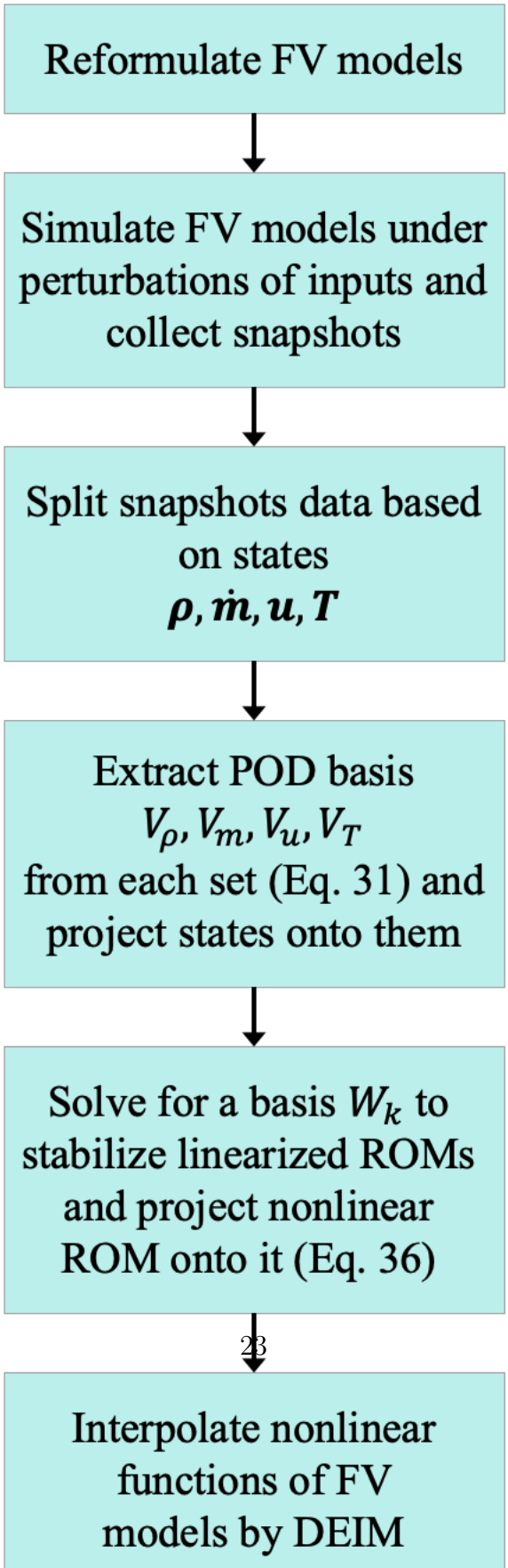
Reformulate FV models
Simulate FV models under perturbations of inputs and collect snapshots
Split snapshots data based on states
$\boldsymbol{\rho}, \dot{\boldsymbol{m}}, \boldsymbol{u}, \boldsymbol{T}$
Extract POD basis
V_ρ, V_m, V_u, V_T
from each set (Eq. 31) and project states onto them
Solve for a basis W_k to stabilize linearized ROMs and project nonlinear ROM onto it (Eq. 36)
Interpolate nonlinear functions of FV models by DEIM

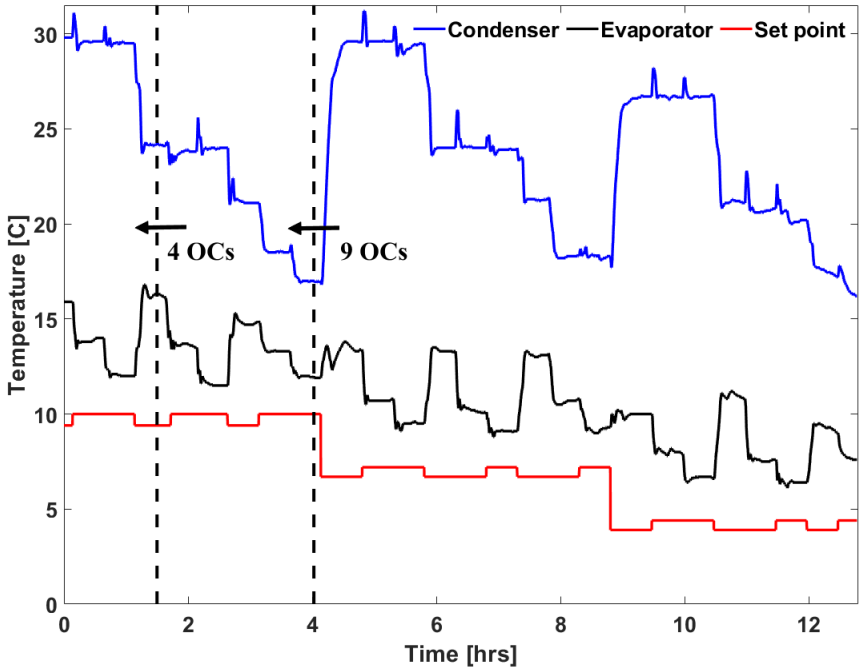

Figure 5: Variations of cycle inputs: water inlet temperatures and the chilled temperature set point

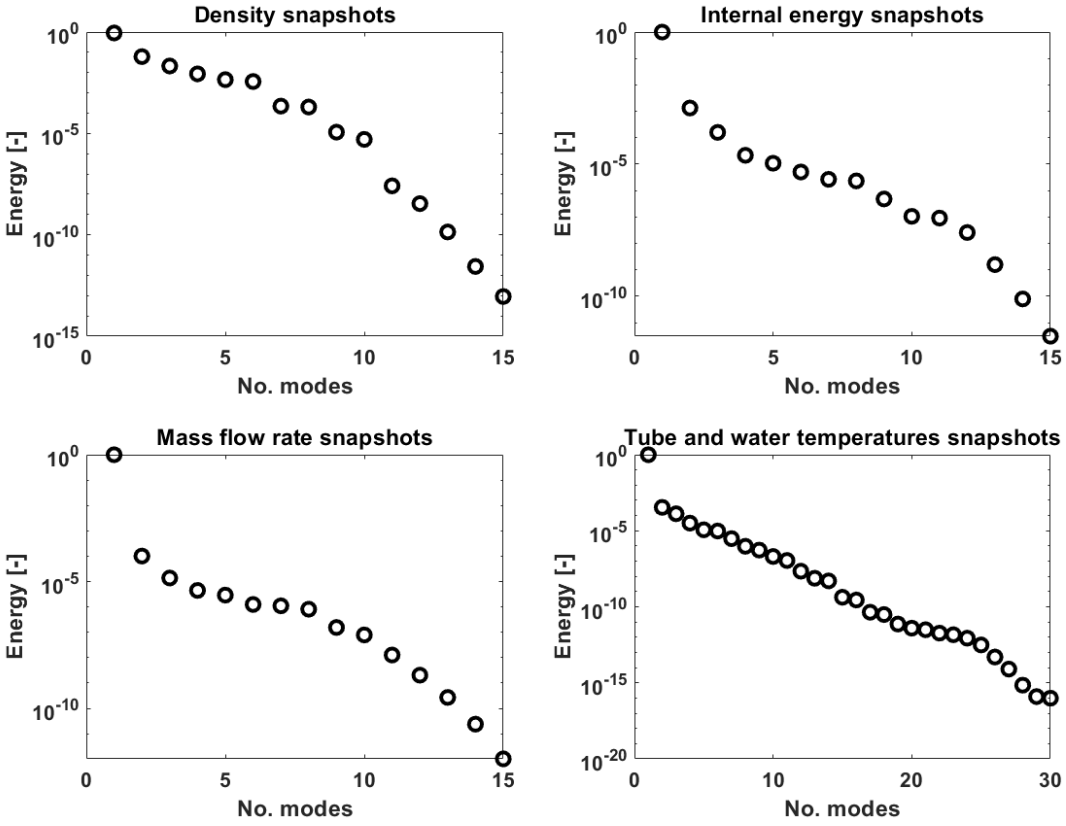

Figure 6: Energy of modes of dynamic states

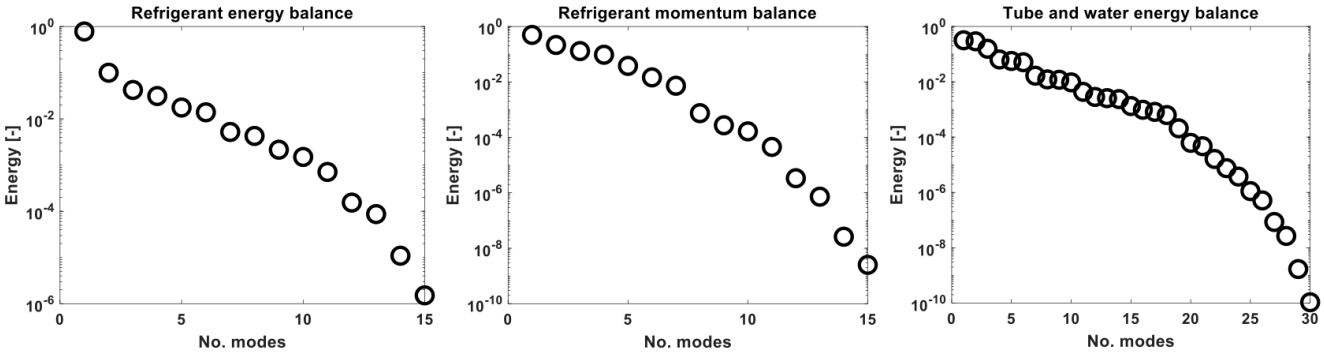

Figure 7: Energy of modes of nonlinear functions

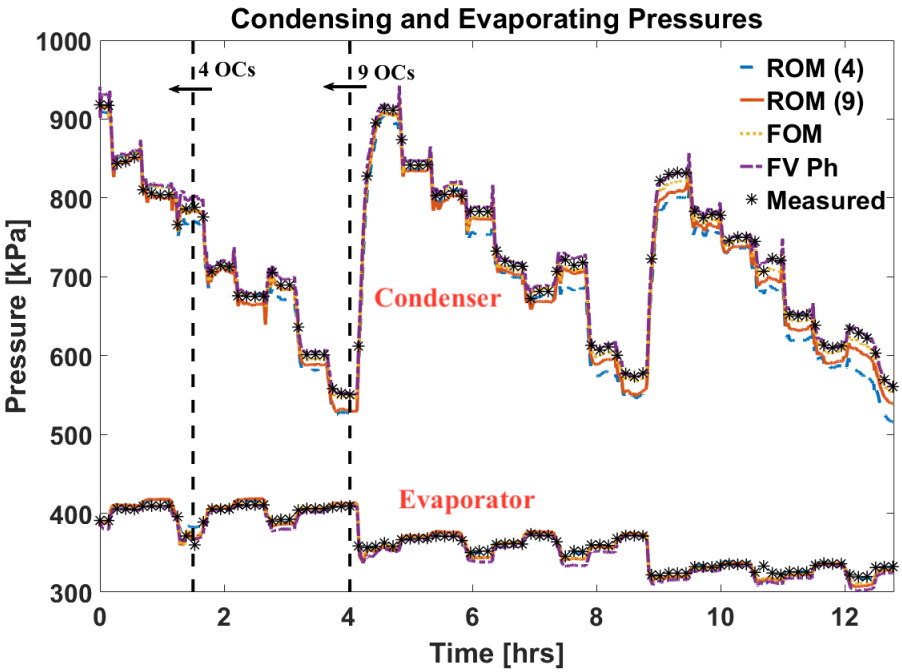

Figure 8: Validations of refrigerant pressures

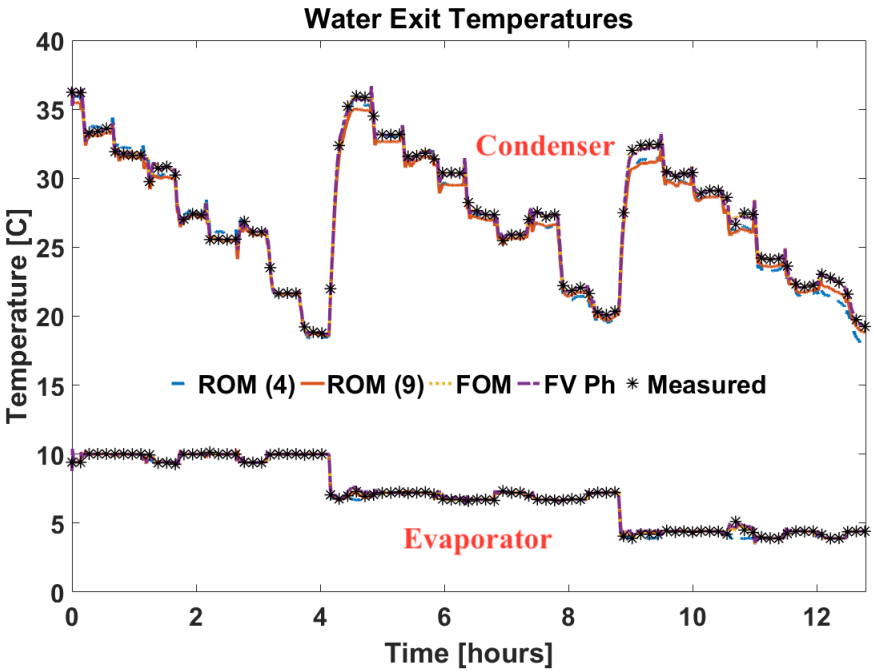

Figure 9: Validations of water exit temperatures

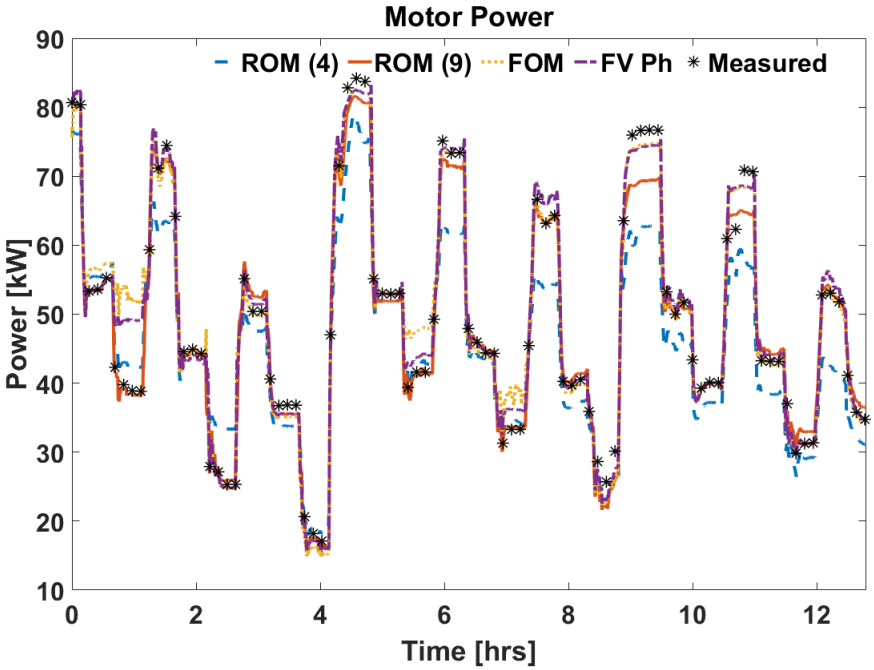

Figure 10: Validations of motor power

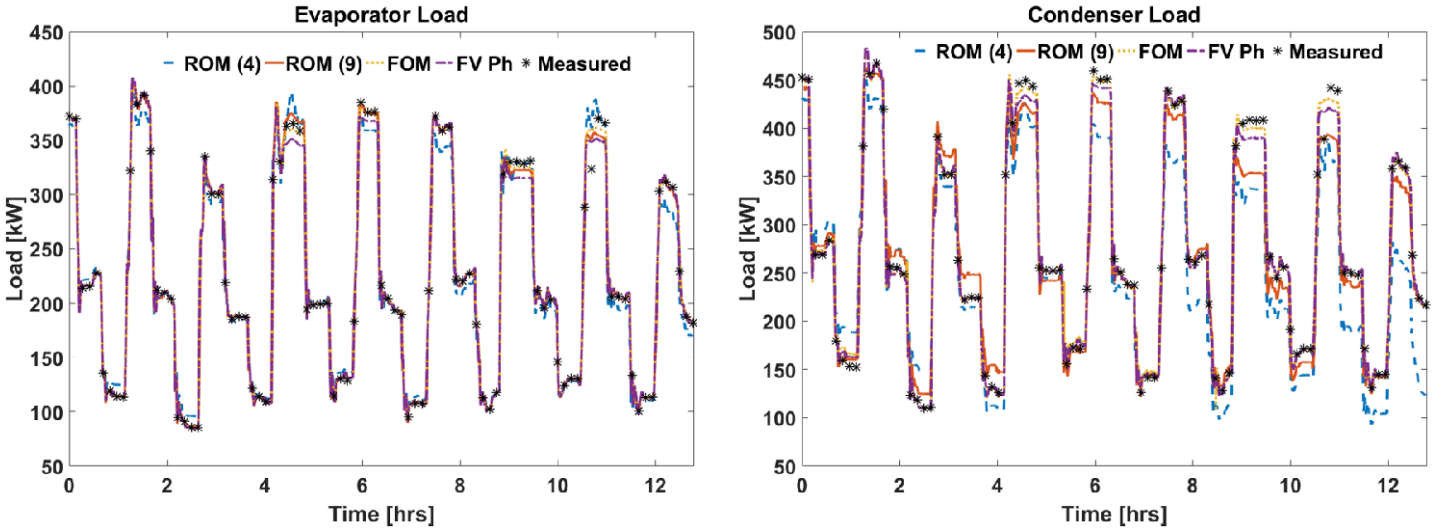

Figure 11: Validations of heat exchanger loads

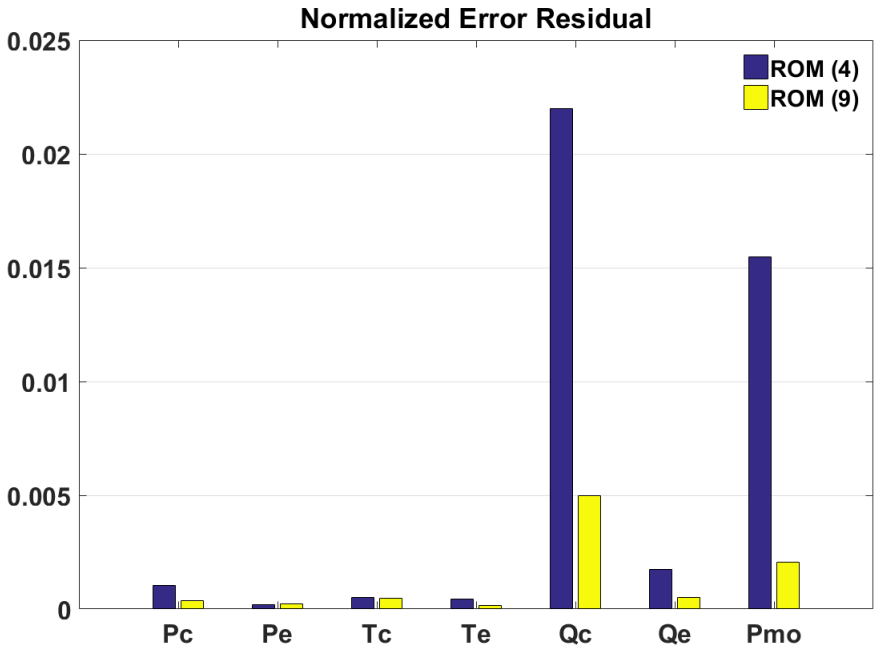

Figure 12: Normalized error residual of ROMs: condensing pressure, evaporating pressure, condenser water exit temperature, evaporator water exit temperature, condenser load, evaporator load, motor power.